PHILOSOPHICAL TRANSACTIONS OF THE ROYAL SOCIETY A MATHEMATICAL, PHYSICAL & ENGINEERING SCIENCES

# Ultrafine particles from combustion sources: approaches to what we want to know

Henning Bockhorn

*Phil. Trans. R. Soc. Lond. A* 2000 **358**, 2659-2672
doi: 10.1098/rsta.2000.0675

10.1098/rsta.2000.0675



# Ultrafine particles from combustion sources: approaches to what we want to know

By Henning Bockhorn

*Institut für Chemische Technik and Engler-Bunte-Institut/Bereich Verbrennungstechnik, Universität Karlsruhe (TH), Kaiserstraße 12, D-76128 Karlsruhe, Germany*

Soot formation and oxidation will be analysed with respect to the most important processes, namely particle inception, coagulation and surface growth. Time-scales of surface growth are estimated for premixed and diffusion flames and compared with time-scales for coagulation. It turns out that characteristic time-scales for soot formation and coagulation are similar and about one order of magnitude larger than the characteristic time-scales for combustion reactions and much smaller than the time-scales of molecular transport.

Coagulation processes will be discussed in detail and a detailed chemistry approach for surface growth will be presented. The detailed information will be put into a soot model that reproduces a number of phenomena in sooting premixed hydrocarbon flames, for example:

(i) the dependence of surface growth and oxidation rates on the chemical 'environment' of soot particles; and

(ii) the fraction of soot formed by particle inception and surface growth reactions and addition of polyacrylic aromatic hydrocarbon (PAH).

The 'fine structure' of soot is not resolved by this approach, and, furthermore, the predictions depend sensitively on information about the kinetics of growth of PAH-like structures, the detailed processes occurring on the surface of soot particles, and, most importantly, the pressure dependence of all these processes.

**Keywords: soot formation; soot oxidation; coagulation; surface growth**

## 1. Introduction

Hydrocarbons tend to form soot when burning under fuel-rich conditions. Soot from combustion of hydrocarbons under fuel-rich conditions appears as an ensemble of ultrafine particles in the size range up to a few hundred nanometres. It is this size range of particles that is suspected to exhibit dangerous effects on human health. Particles of this size easily penetrate into the respiratory tracts and are thought either to stimulate the defence mechanisms similar to that against small fibres or act via chemical compounds adsorbed on the surface of the particles.

The formation of soot, i.e. the conversion of a hydrocarbon fuel molecule containing few carbon atoms into a carbonaceous agglomerate containing some millions of carbon atoms, is an extremely complicated process. It is a kind of gaseous–solid

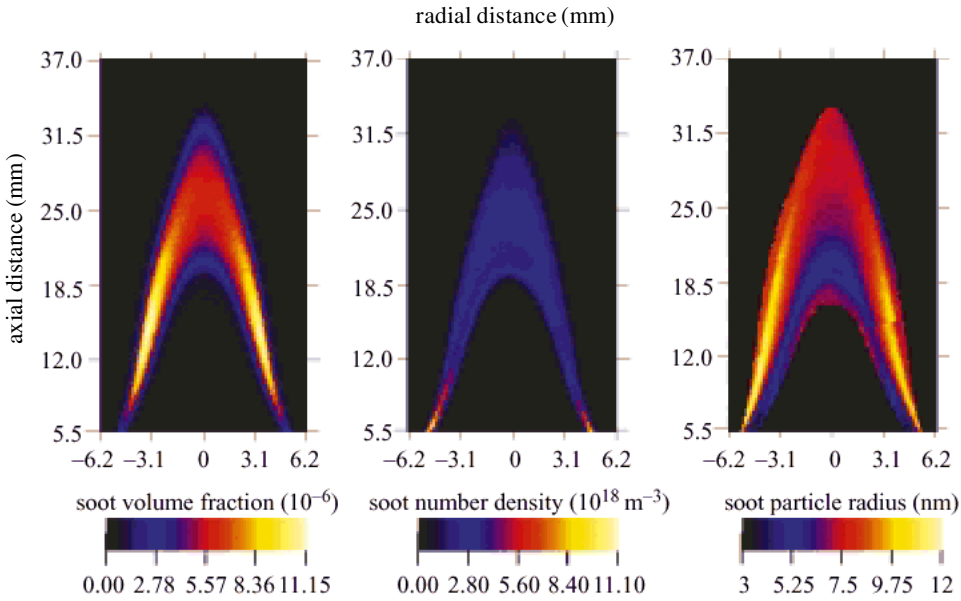


Figure 1. Two-dimensional maps of particle number density $N_V$, soot volume fraction $f_V$, and mean particle radius $r_m$ of a laminar acetylene–air diffusion flame, fuel diluted with nitrogen.

phase transition where the solid phase exhibits no unique chemical and physical structure. Therefore, soot formation encompasses chemically and physically different processes, e.g. the formation and growth of large aromatic hydrocarbons and their transition to particles, the coagulation of primary particles to larger aggregates, and the growth of solid particles by picking up growth components from the gas phase. The above-mentioned processes constitute the formation of the bulk of soot. In addition, numerous other processes decide on the 'fine structure' of soot, e.g. the formation of electrically charged soot particles, the formation—charged and neutral—of fullerenes, or the formation of high molecular weight tarry modifications with optical properties quite different from carbon black, and a variety of modifications of soot with different optical and mechanical properties.

While much progress has been achieved in understanding all these processes, numerous problems remain unsolved. In the following, some recent development in mechanisms and models of soot formation will be discussed, focusing on processes of the formation of the bulk of soot and attempting to reduce the gap for a comprehensive understanding of soot formation.

## 2. Structure of sooting flames

The locally resolved structure of laminar and turbulent sooting diffusion flames with respect to soot volume fractions $f_V$, particle number densities $N_V$ and particle sizes $r_m$ has recently been investigated by Geitlinger *et al.* (1998, 1999) by means of a two-dimensional imaging technique employing a combination of Rayleigh scattering and laser-induced incandescence (LII).

Figure 1 gives, as an example from the above-referenced work, two-dimensional maps of soot volume fractions $f_V$, particle number densities $N_V$ and particle sizes

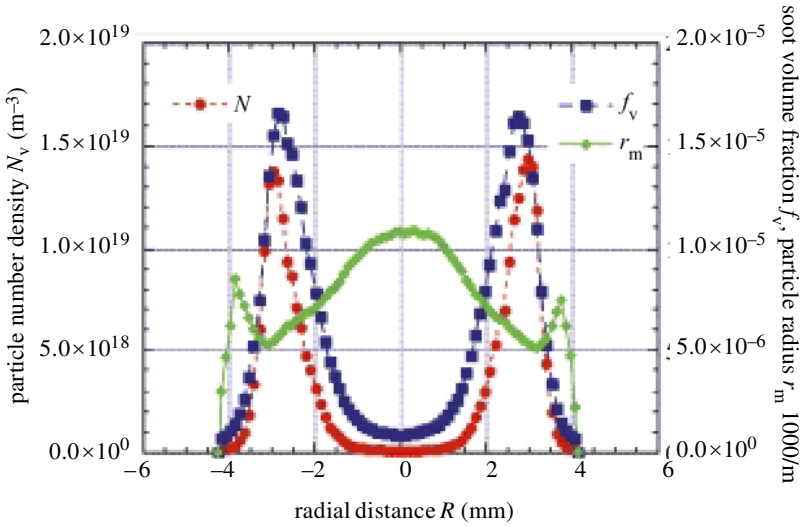


Figure 2. Profiles of particle number density $N_V$, soot volume fraction $f_V$, and mean particle radius $r_m$ of the laminar acetylene–air diffusion flame from figure 1 at 15 mm height above the burner nozzle.

$r_m$ of a bunsen-type, laminar acetylene–air diffusion flame, the fuel of which is diluted with nitrogen. The corresponding profiles at 15 mm height above the burner nozzle are displayed in figure 2.

The figures clearly show that at low heights no soot can be observed in the centre of the flame. At the radial position of the maximum in $N_V$, a minimum in the particle size appears. The soot formation zone is located at this radial position, where particle inception prevails, generating a large number of small particles. The maximum in the soot volume fraction $f_V$ occurs at somewhat smaller radial distances, indicating that surface growth reactions are taking place in the preheating zone of the fuel, where temperatures are still high enough for this process. Surface growth reactions add mass to the small particles being formed in the particle-inception region. Towards lower radial distances, $r_m$ increases because of surface growth reactions as well as coagulation. The latter process—which adds no mass to the particles but changes their size drastically—is very fast, indicated by the strong decrease in $N_V$ towards lower radial distances. The apparent increase in $r_m$ towards the oxygen-rich zone of the diffusion flame can be explained by coagulation of soot particles as well as the complete oxidation of the smallest soot particles in the reaction zone of the flame. All the profiles exhibit steep gradients when moving towards the oxidation zone of the flame.

At larger heights above the burner in the cone-shaped flame, the profiles are moving towards the centre of the flame. The largest particles are then observed in the centre of the flame. At this position $f_V$ is quite low and the particle radii are dominated by coagulation. At the tip of the sooting region the profiles of $f_V$ and $N_V$ from each side of the flame are fusing together. For $f_V$ no minimum can be observed in the centre of the flame. The maxima in $f_V$ and $N_V$ decrease because of the consumption of soot when reaching the oxidation zone at the flame tip. Particle number density is of the order of $1 \times 10^{18}$ m$^{-3}$, whereas mean particle sizes are of the order of 20 nm and soot volume fractions are *ca.* 20 ppm.

Besides the orders of magnitude for $N_V$, $f_V$ and $r_m$ in diffusion flames of that kind, from the above figures the different main processes leading to the final soot particle ensemble can be identified. These processes can be summarized roughly as follows:

(i) formation of primary soot particles (particle inception),

(ii) surface growth reactions of soot particles, and

(iii) coagulation of soot particles.

These processes are discussed in more detail in the subsequent sections.

## 3. Processes leading to soot

### (a) *Coagulation processes*

The first and third of the above processes comprise (reactive) coagulation processes, where particles (molecules) of size $i$ collide with those of size $j$. These processes can be uniquely described by coagulation kinetics.

For a coagulating particle system the change of number density for particles of the size class $i$ with time is given by the Smoluchowsky equation

$$\frac{\mathrm{d}N_i}{\mathrm{d}t} = \frac{1}{2}\sum_{j=1}^{i-1}\beta_{j,i-j}N_jN_{i-j} - N_i\sum_{j=1}^{n_{\max}}\beta_{i,j}N_j, \quad i = 2,\ldots,n_{\max}. \tag{3.1}$$

In equation (3.1), $N_i$ and $N_j$ represent the number density of particles in the size class $i$ and $j$, respectively. The coagulation coefficient $\beta_{i,j}$ for free molecular coagulation is given by

$$\beta_{i,j} = \sqrt{\frac{8\pi k_B T}{\mu_{i,j}}}(r_i + r_j)^2 = C\sqrt{\frac{1}{i} + \frac{1}{j}}(i^{1/3} + j^{1/3})^2, \tag{3.2}$$

where

$$C = \sqrt{\frac{8\pi k_B T}{m_1}}\left(\frac{3m_1}{4\pi\rho}\right)^{2/3}. \tag{3.3}$$

The first term on the right-hand side of equation (3.1) gives the formation rate of particles in the size class $i$ by coagulation of smaller particles, the sizes of which add to the size $i$, whereas the second term describes the consumption rate of particles in the size class $i$ by collision with other particles. To include addition of large hydrocarbons to the surface of soot particles by sticky collisions, they have to be included in the system of equations (3.1), while the formation rates of those obey different mechanisms. The smallest particles, the sizes of which are defined so as to consist of two pyrene molecules (Appel & Bockhorn 2000), are balanced by

$$\frac{\mathrm{d}N_1}{\mathrm{d}t} = \tfrac{1}{2}\beta_{0,1}N_0^2 - N_1\sum_{j=1}^{n_{\max}}\beta_{1,j}N_j, \tag{3.4}$$

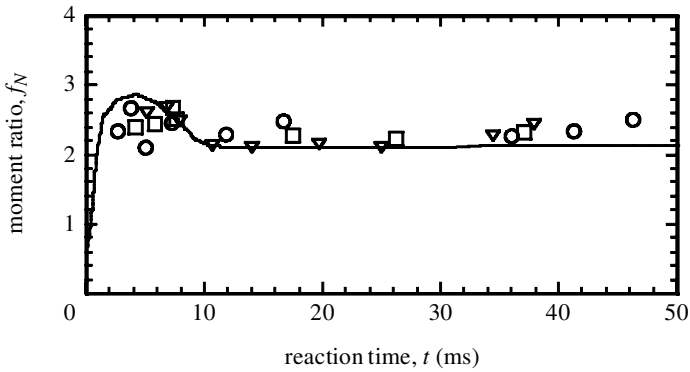


Figure 3. Evolution of the moment ratio $f_N = \mu_6/\mu_3^2$ for different low-pressure premixed flames (Bockhorn *et al.* 1987); symbols refer to TEM measurements, the solid line denotes the numerical solution of the coagulation equation with particle inception being modelled to produce 5% of the total soot mass within the first 3 ms of soot formation. ∇, propane; ○, benzene; □, acetylene; ——, calculated.

where $N_0$ is the number density of the last pre-particle species. Again, particle number densities $N_0$ have to be obtained from different considerations. The Schmoluchowsky equation written for the total particle number density,

$$N = \sum_i N_i,$$

gives

$$\frac{\mathrm{d}N}{\mathrm{d}t} = -\tfrac{1}{2}\beta(i)N^2, \tag{3.5}$$

where $\beta(i)$ is a weak function of the particle size. Assuming $\beta(i)$ to be independent of particle size, then $\beta \approx 10^{-16}\ \mathrm{m^3\ s^{-1}}$ at 2000 K, and a particle number density of *ca.* $10^{18}\ \mathrm{m^{-3}}$ results in coagulation rates of *ca.* $10^{20}\ \mathrm{m^{-3}\ s^{-1}}$ or characteristic time-scales for coagulation of $\tau_{\mathrm{coag}} \approx 10$ ms. At incipient soot formation, number densities exceed those in the surface growth region (cf. figure 2), so that characteristic time-scales for coagulation are even smaller and attain similar values to characteristic time-scales for combustion reactions.

With $\beta \approx$ const., the solution of equation (3.5) results in

$$N = \frac{N_0}{1 + N_0\beta t} = \frac{1}{(1/N_0) + \beta t}. \tag{3.6}$$

For $\beta t \gg (1/N_0)$, it follows that $N \propto (1/\beta t)$. For comparatively long coagulation times the number density is no longer dependent on initial conditions $N_0$ and is only given by $\beta$ and $t$. The particle ensemble loses its memory and, for typical conditions in flames (temperature 2000 K, $\beta \approx 10^{-16}\ \mathrm{m^3\ s^{-1}}$, coagulation time 100 ms), particle number densities of *ca.* $10^{17}\ \mathrm{m^{-3}}$ are attained. When emitted with the exhaust, particle number density and particle sizes of the soot particle aerosol 'in accumulation mode' exhibit a broad size distribution with low particle number densities, which change only slowly. In contrast, soot particle aerosols in 'nucleation mode' show narrow size distributions with high number densities.

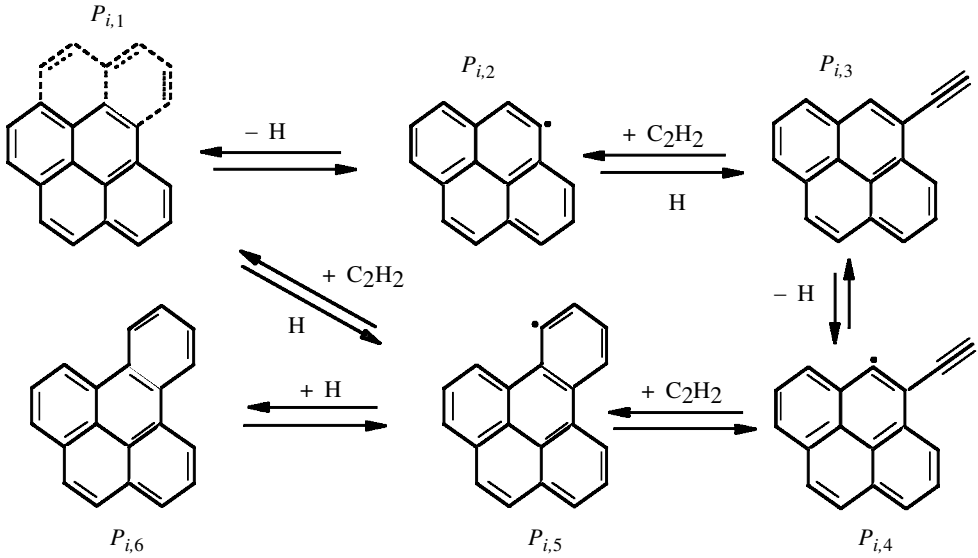


Figure 4. HACA mechanism for the surface growth of soot (Frenklach & Wang 1994).

The properties of a coagulating particle system are independent of the initial conditions (after sufficiently large reaction times). Another consequence of this is the evolution of a 'self-preserving' size distribution of the particle ensemble. 'Self-preserving' means that moment ratios of the size distribution $P(r)$ remain constant, e.g. $f_N \equiv (\mu_6/\mu_3^2) = 2.079$, where

$$\mu_i = \int_0^\infty r^i P(r)\,\mathrm{d}r$$

are the moments of the particle size distribution. When increasing the mean particle size by coagulation, the variances of soot particle size distributions, therefore, increase. The evolution of the moment ratio $f_N = \mu_6/\mu_3^2$ for different premixed, low-pressure flames is given in figure 3 (Bockhorn *et al.* 1987) and compared with modelling. For modelling, the appropriate term for the change of number densities in the different size classes by surface growth has been added to equation (3.1) (cf. Bockhorn *et al.* 1985, 1987). The figure demonstrates that the theoretical value of the moment ratio is quickly attained, and, from the good agreement between measured and simulated values, one can conclude that in flames the largest part of soot is formed by surface growth reactions (more than 95%), rather than by particle inception, and that particle inception occurs to a large extent only during the first few milliseconds of the process. A similar picture is obtained for diffusion flames (cf. figures 1 and 2) for the particle inception and coagulation region that are tied down by the mixing of fuel and oxidant. When crossing the oxidation zone in diffusion flames, particle size distributions change their shape, because smaller particles are consumed first by oxidation and the larger ones resist complete burn-out for longer.

### (*b*) *Surface growth processes*

If the major proportion of soot is formed by surface growth reactions, the formation of the bulk of soot is well described via surface growth. Surface growth of soot

Table 1. *Surface growth reactions for soot particles (after Schäfer et al. 1995)*

| | | | | | | |
|---|---|---|---|---|---|---|
| (1a) | $C_{soot,i}H$ | + H | $\overset{k_{1a,s}}{\rightleftharpoons}$ | $C^*_{soot,i}$ | + $H_2$ |
| (1b) | $C_{soot,i}H$ | + OH | $\overset{k_{1b,s}}{\rightleftharpoons}$ | $C^*_{soot,i}$ | + $H_2O$ |
| (2) | $C^*_{soot,i}$ | + H | $\overset{k_{2,s}}{\rightarrow}$ | $C_{soot,i}H$ | | |
| (3a) | $C^*_{soot,i}$ | + $C_2H_2$ | $\overset{k_{3a,s}}{\rightleftharpoons}$ | $C^*_{soot,i}C_2H_2$ | | |
| (3b) | $C^*_{soot,i}C_2H_2$ | | $\overset{k_{3b,s}}{\rightleftharpoons}$ | $C_{soot,i+1}H$ | + H |
| (4a) | $C^*_{soot,i}$ | + $O_2$ | $\overset{k_{4a,s}}{\rightarrow}$ | $C^*_{soot,i-1}$ | + 2CO |
| (4b) | $C^*_{soot,i}C_2H_2$ | + $O_2$ | $\overset{k_{4b,s}}{\rightarrow}$ | $C^*_{soot,i}$ | + 2CHO |
| (5) | $C_{soot,i}H$ | + OH | $\overset{k_{5,s}}{\rightarrow}$ | $C^*_{soot,i-1}$ | + CH + CHO |

has been interpreted in terms of the active site model (Woods & Hanyes 1994) as well as the acetylene decomposition model (Harris & Weiner 1990). These explanations provide a chemical interpretation of the appearance rates of soot via the decomposition of acetylene at active sites on the soot particle surface and via the deactivation or thermal stabilization of surface growth sites. The resulting rate expressions are of first order in the partial pressure of acetylene. A mechanistic interpretation of surface growth has been introduced by Frenklach (see, for example, Frenklach & Wang 1994). The basic idea of this approach, which has been adopted meanwhile in numerous works, is the transfer of the H abstraction carbon-addition (HACA) mechanism for the planar growth of polyacrylic aromatic hydrocarbon (PAH) to the heterogeneous surface growth of soot particles. The HACA mechanism provides a linear replication scheme for the planar growth of PAH by a two-step H-abstraction $C_2H_2$-addition (cf. figure 4). In this approach, PAH growth encompasses reactions between similar classes of particles so that the complex mixture may be described by lumped species classes rather than by single PAH species.

This approach is transferred to the surface growth of soot particles, which represent a weak-interaction cluster of PAH molecules (cf. table 1). In the reaction scheme given in table 1, $C_{soot}H$ represents an armchair site on the soot particle and $C^*_{soot}$ the corresponding radical. $S$ is the surface area of the soot particles and $\chi(C_{soot}H)$ is the number of CH sites per unit surface area accessible for surface growth. This formulation does not necessarily restrict surface growth to the outer surface of soot particles. If 'soot radicals' are replaced by the assumption of quasi-stationarity, the appearance rates of soot can be reproduced by

$$\frac{\mathrm{d}f_V}{\mathrm{d}t} \propto \left( \frac{k_{1a,f}[H]k_{4a}[O_2] \cdot ((k_w[C_2H_2]/k_{4a}[O_2]) - 1)}{k_{1a,b}[H_2]} - k_5[OH] \right) \chi(C_{soot}H)S. \quad (3.7)$$

Further assumptions applied to derive equation (3.7) are that the growth mechanism is mainly initiated by H abstraction from the attack of H via reaction (1a) (see table 1), that the consumption of $C^*_{soot,i}$ is dominated by the reverse of reaction (1a) and that the rate coefficients for $C_2H_2$ addition ($k_{3a,f}$), $C_2H_2$ abstraction ($k_{3a,b}$) and ring closure ($k_{3b,f}$) are lumped into $k_w$.

Equation (3.7) reveals that only if $k_w[C_2H_2]/k_{4a}[O_2] \gg 1$ are the surface growth rates are of first order in the acetylene concentration. For this case, where surface

growth reactions are dominating, the appearance rates are controlled by the ratio of [H]:[$H_2$]. The development of this concentration ratio and of the temperature in the soot-formation region is then responsible for the course of the appearance rates of soot. If oxidation is more important, i.e. if $k_w[C_2H_2]/k_{4a}[O_2] \approx 1$ and if $k_5$[OH] is not negligible, the appearance rates follow a more complicated concentration dependence. For most flame conditions $k_w[C_2H_2]/k_{4a}[O_2] \gg 1$. Therefore, for the conditions in most flames the rate of acetylene addition dominates, so that the soot-formation rate is mostly of first order in the concentration of acetylene.

## 4. Modelling of soot formation and oxidation

When modelling soot formation and oxidation employing the principal processes outlined above, soot formation and oxidation is embedded into the detailed description with the help of the gas-phase chemistry that provides H atom and acetylene concentrations, formation and growth of PAH, and formation and growth of soot particles by particle inception, surface growth and other collision processes. For numerical simulation the mass balances for all of the involved chemical species (about 250 chemical species and 1200 chemical reactions) and the enthalpy balance have to be solved.† The soot particle phase is treated as the balance equations of the moments of the size distribution (Frenklach & Wang 1994; Mauß *et al*. 1994; Mauß & Bockhorn 1995), which leads to a closed system of equations. Details of the modelling and numerical methods can be found in Frenklach & Wang (1994), Frenklach & Harris (1987) and Mauß & Bockhorn (1995).

Some results from the application of the above sketched modelling approach are plotted in figures 5 and 6. Figure 5 gives a comparison of the calculated and measured soot volume fractions for a premixed, flat acetylene–oxygen flame. In addition, the different contributions to the soot appearance rates—namely, particle inception, surface growth, PAH addition, as well as oxidation by oxygen and OH radicals—are indicated. The figure clearly demonstrates that

(i) the experimentally measured soot volume fractions can be predicted well for that flame,

(ii) the most important contribution to soot comes from surface growth, and

(iii) other processes contribute only a little.

Obviously, oxidation by OH takes place simultaneously during the entire soot-formation process, while oxidation by $O_2$ is of minor importance for the prevailing experimental conditions.

Figure 6 demonstrates the applicability of the model in a wide range of experimental conditions and for different fuels. The experimental conditions of the flames, the experimentally measured soot volume fraction profiles of which are compared with the corresponding calculations in figure 6, are given in table 2. The model used for this comparison has been modified slightly compared with the concept outlined above (for details see Appel *et al*. (2000)). The figure reveals generally very good agreement between measurements and calculations. Note that the soot volume fractions in the considered flames vary by some orders of magnitude.

† For the formulation of the corresponding balance equations, see, for example, Gardiner (1984) and Warnatz *et al*. (1996).

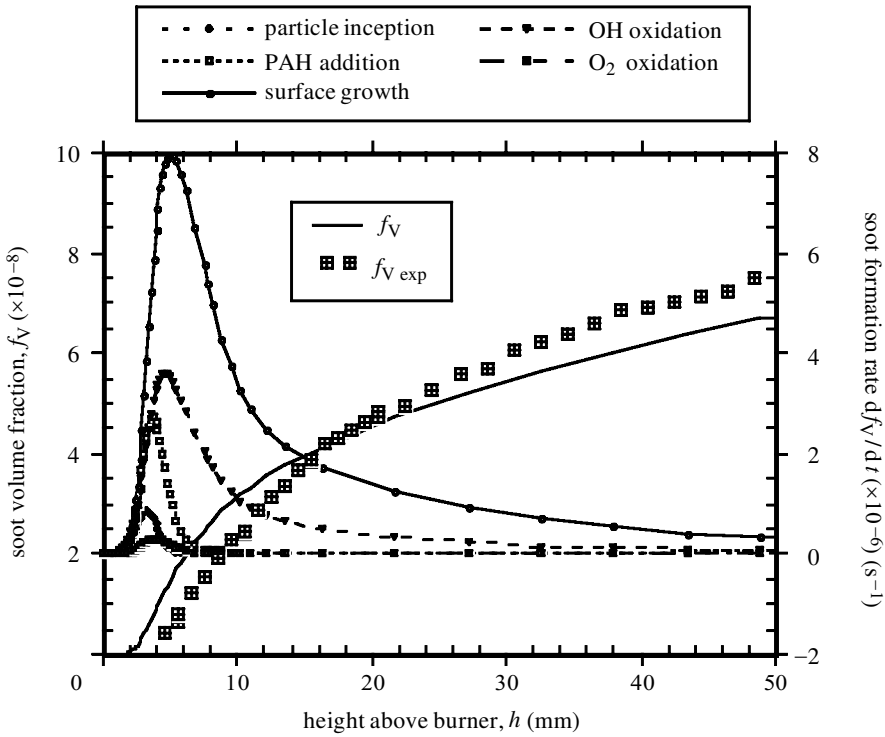


Figure 5. Measured and calculated soot volume fractions for a premixed acetylene–oxygen–argon flame. Initial conditions: $T = 298$ K; $P = 12$ kPa; C:O ratio 1.25; and Ar 60%.

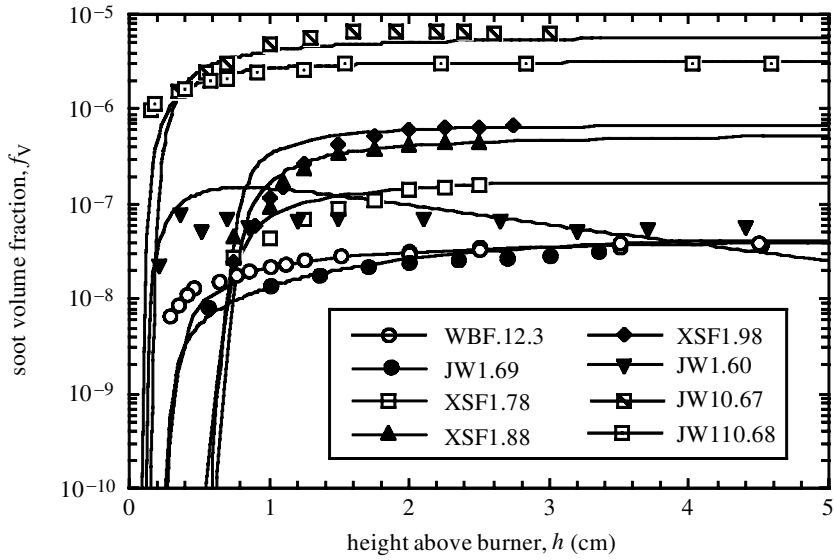


Figure 6. Measured and calculated soot volume fractions for premixed hydrocarbon flames (from Appel *et al.* 2000). For experimental conditions see table 2.

Table 2. *Experimental conditions for the flames given in figure 6*

| flame | fuel | fuel (mol %) | $O_2$ (mol %) | $N_2$ or Ar (mol %) | $v$ (cm $s^{-1}$) | C/O | $T_{max}$ (K) | $P$ (bar) |
|---|---|---|---|---|---|---|---|---|
| WBF.12.3 | $C_2H_2$ | 22.6 | 12.4 | 55.0 (Ar) | 20.1 | 1.3 | 1992 | 0.12 |
| JW1.69 | $C_2H_4$ | 12.66 | 18.34 | 69.0 ($N_2$) | 5.9 | 0.69 | 1711 | 1.013 |
| XSF1.78 | $C_2H_4$ | 14.0 | 18.0 | 68.0 ($N_2$) | 4.0 | 0.78 | 2104 | 1.013 |
| XSF1.88 | $C_2H_4$ | 15.5 | 17.4 | 67.1 ($N_2$) | 6.9 | 0.88 | 1957 | 1.013 |
| XSF1.98 | $C_2H_4$ | 17.0 | 17.4 | 65.6 ($N_2$) | 5.3 | 0.98 | 1908 | 1.013 |
| CS1.748 | $C_2H_6$ | 24.12 | 32.25 | 43.36 (Ar) | 7.0 | 0.748 | 1270 | 1.013 |
| JW10.60 | $C_2H_4$ | 11.2 | 18.65 | 70.15 ($N_2$) | 6.0 | 0.60 | 2017 | 10 |
| JW10.67 | $C_2H_4$ | 12.38 | 18.40 | 69.22 ($N_2$) | 3.0 | 0.673 | 1895 | 10 |
| JW10.68 | $C_2H_4$ | 12.5 | 18.40 | 69.1 ($N_2$) | 6.0 | 0.68 | 1880 | 10 |

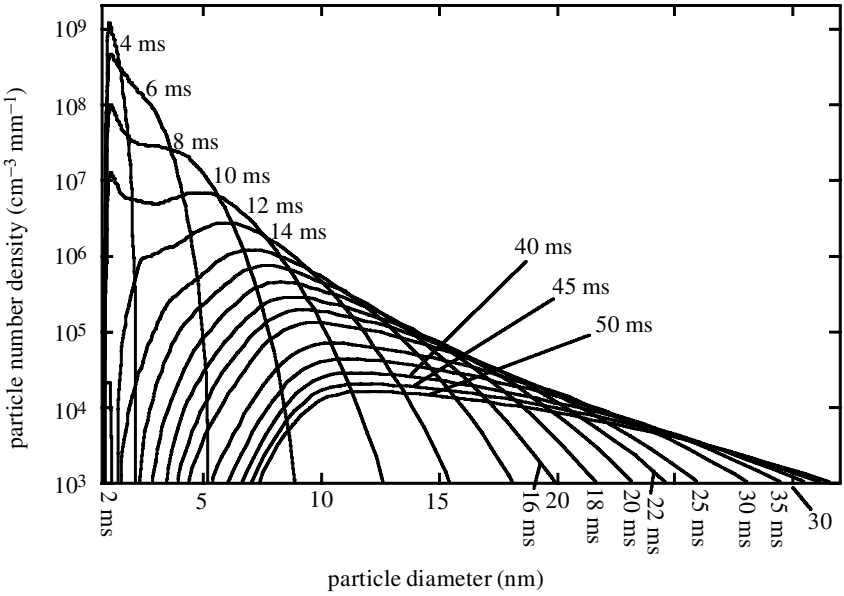


Figure 7. Evolution of the soot particle size distributions for a premixed, low-pressure propane–oxygen flame (Bockhorn *et al*. 1983).

Finally, the simulated full particle size distribution is depicted in figure 7 for a premixed, low-pressure propane–oxygen flame from Bockhorn *et al*. (1983). The computations have been performed by solving the coagulation equations of the form

$$\frac{\mathrm{d}N_i}{\mathrm{d}t} = f(N_1, N_2, \ldots, N_m), \qquad i = 1, 2, \ldots, m. \tag{4.1}$$

In equation (4.1) $N_i$ is the number density of particles, which are built up from $i$ monomer units. The right-hand side of equation (4.1) contains all processes that

Figure 8. Comparison of experimental and calculated soot particle size distributions. The relative number of particles in the experiment is the number of particles of a certain size divided by the total number of examined particles. Due to the experimental technique used in Bockhorn *et al*. (1988), a comparison of absolute numbers is not possible.

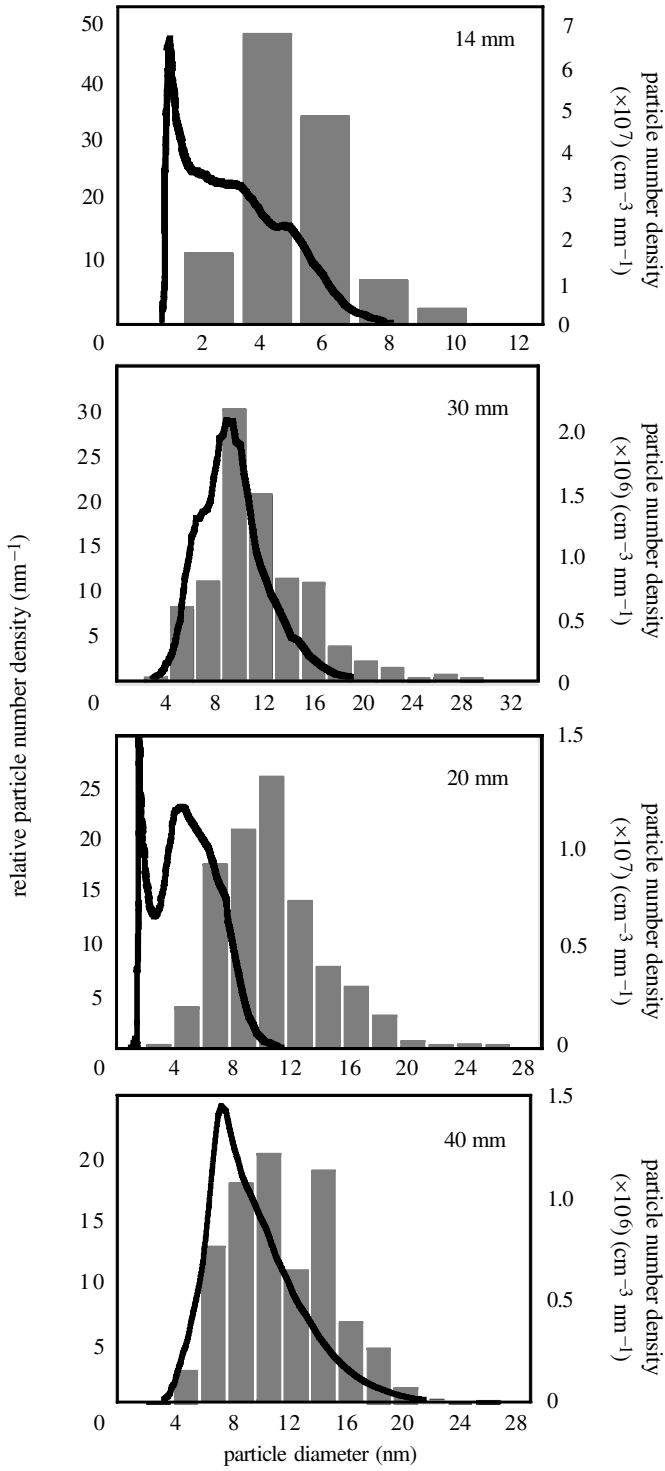


Figure 8. For description see opposite.




PHILOSOPHICAL TRANSACTIONS OF THE ROYAL SOCIETY A MATHEMATICAL, PHYSICAL & ENGINEERING SCIENCES

contribute to the size evolution of the soot particle aerosol, namely particle inception, coagulation, surface growth and deposition of aromatic hydrocarbons at the surface of the soot particles. The algorithm used approximates the size distributions by a multilevel Galerkin h-p-method (Wulkow 1996). The calculation is post-processed after numerical simulation of the complete structure of the premixed flame (Appel & Bockhorn 2000). From the evolution of the soot particle size distributions it can be seen that particle inception and coagulation still dominate the particle dynamics of the system. Surface growth affects the distribution in the main reaction zone. In this region the main amount of soot is added to the solid phase by heterogeneous surface reactions with acetylene. The width of the distribution increases rapidly during this process (cf. figure 7). After the narrow surface growth zone, coagulation is again the dominant source for the evolution of the particle size distribution.

The rate of surface growth is proportional to a fraction of the surface area of the soot particles (see equation (3.7)). If the particles are assumed to be spherical, the surface area of a particle can be determined by

$$S_i = 4\pi \left( \frac{3m_1}{4\pi\rho_{\mathrm{soot}}} \right)^{2/3} i^{2/3}, \tag{4.2}$$

and the diameter of the particles is given by

$$d_i = 2 \left( \frac{3m_1}{4\pi\rho_{\mathrm{soot}}} \right)^{1/3} i^{1/3}. \tag{4.3}$$

The two major processes in soot particle dynamics, namely coagulation and surface growth, have a strong size dependence. For coagulation, high coagulation rates are obtained for the collisions of small particles with large ones, due to the size dependence of the mean velocity of the particles and the collisional cross-sections. This causes a fast consumption of small particles. The size dependence of the rates of surface growth reactions implies that the rate of acetylene addition is high for large particles. However, due to the size dependence of the ratio of surface area to diameter, in regions with many small particles the specific surface area is high and so the overall soot growth rate is also high.

Finally, in figure 8 a comparison of the computed particle size distributions with experimentally determined distributions (Bockhorn *et al.* 1988) is presented. The experimental results are obtained from molecular beam sampling of the sooting flame and TEM micrographs of the soot particles. The experimental values are relative particle number densities, which indicate the percentage of particles, which were found within a certain range of diameters. The lower detection limit of the experiments was reported to be *ca.* 1 nm. At low heights above the burner, the calculated soot particle size distributions show smaller particles than in the experimental observations. This can be explained by experimental uncertainties, because of the difficulty of extracting the particles from the main reaction zone of the flame. The agreement between the simulated and measured size distributions at 30 and 40 mm above the burner is excellent.

## 5. Summary

In the preceding sections, soot formation and oxidation have been analysed with respect to the most important processes, namely particle inception, coagulation and

surface growth. Time-scales for surface growth, $\tau_{\mathrm{soot}} < 10$ ms, can be estimated for premixed flames that are comparable with the time-scales for soot formation in diffusion flames. Time-scales for coagulation are estimated as $\tau_{\mathrm{coag}} \approx 10$ ms, so that characteristic time-scales for soot formation and coagulation are similar and about one order of magnitude larger than the characteristic time-scales for combustion reactions. Obviously, the time-scales for soot formation and oxidation for the prevailing conditions in most flames are small compared with the time-scales of molecular transport, so that the soot appearance rates are adjusted to the local flame conditions.

In summary, one can conclude that the approach discussed above for a detailed chemistry soot model reproduces a number of phenomena in sooting premixed hydrocarbon flames, e.g.

(i) the dependence of surface growth and oxidation rates on chemical 'environment' of soot particles, and

(ii) the fraction of soot formed by particle inception and surface growth reactions and addition of PAH.

In addition, the model identifies time-scales of soot formation, soot oxidation and coagulation that are larger than the time-scales of combustion reactions, but are smaller than the time-scales of molecular or turbulent transport. Consequently, 'fast-chemistry' models can be employed when modelling soot formation and oxidation in more complex geometries.

However, the 'fine structure' of soot is not resolved by this approach, e.g.

(i) formation of charged soot particles,

(ii) formation of species such as fullerenes, charged and uncharged, and

(iii) formation of 'non-absorbing soot' that may play a role at incipient soot formation (d'Anna *et al*. 1994).

Furthermore, much more information about the kinetics of growth of PAH-like structures (growth reactions may be size dependent), the detailed processes occurring on the surface of soot particles, and, most importantly, the pressure dependence of all these processes is necessary to extend the validity of this approach to a wider range of experimental conditions.

## References

Appel, J. & Bockhorn, H. 2000 *Chemosphere*. (In the press.)

Appel, J., Bockhorn, H. & Frenklach, M. 2000 *Combust. Flame* **121**, 122.

Bockhorn, H., Fetting, F. & Wenz, H. W. 1983 *Ber. Bunsenges. Phys. Chem.* **87**, 1067.

Bockhorn, H., Fetting, F., Heddrich, A. & Wannemacher, G. 1985 In *20th Symp. (Int.) on Combustion*, p. 979. Pittsburgh, PA: The Combustion Institute.

Bockhorn, H., Fetting, F., Heddrich, A. & Wannemacher, G. 1987 *Ber. Bunsenges. Phys. Chem.* **91**, 819.

Bockhorn, H., Fetting, F., Heddrich, A., Meyer, U. & Wannemacher, G. 1988 *J. Aerosol Sci.* **19**, 591.

d'Anna, A., d'Alessio, A. & Minutulo, P. 1994 In *Soot formation in combustion—mechanisms and models* (ed. H. Bockhorn), p. 83. Springer.

Frenklach, M. & Harris, S. J. 1987 *J. Colloid Interface Sci.* **118**, 252.

Frenklach, M. & Wang, H. 1994 In *Soot formation in combustion—mechanisms and models* (ed. H. Bockhorn), p. 165. Springer.

Gardiner, W. C. (ed.) 1984 *Combustion chemistry*. Springer.

Geitlinger, H., Streibel, Th., Suntz, R. & Bockhorn, H. 1998 In *27th Symp. (Int.) on Combustion*, p. 1613. Pittsburgh, PA: The Combustion Institute.

Geitlinger, H., Streibel, Th., Suntz, R. & Bockhorn, H. 1999 *Combust. Sci. Technol.* **149**, 115.

Harris, S. J. & Weiner, A. 1990 *Combust. Sci. Technol.* **72**, 67.

Mauß, F. & Bockhorn, H. 1995 *Z. Phys. Chem.* **188**, 45.

Mauß, F., Trilken, B., Breitbach, H. & Peters, N. 1994 In *Soot formation in combustion—mechanisms and models* (ed. H. Bockhorn), p. 325. Springer.

Schäfer, Th., Mauß, F., Bockhorn, H. & Fetting, F. 1995 *Z. Naturf.* **50a**, 1009.

Warnatz, J., Maas, U. & Dibble, R. W. 1996 *Combustion*. Springer.

Woods, I. T. & Haynes, B. S. 1994 In *Soot formation in combustion—mechanisms and models* (ed. H. Bockhorn), p. 275. Springer.

Wulkow, M. 1996 *Macromol. Theory Simul.* **5**, 393.